Journal of
MATERIALS RESEARCH

Titania and silica powders produced in a counterflow diffusion flame

Aaron J. Rulison,[a] Philippe F. Miquel,[b] and Joseph L. Katz[c]
Department of Chemical Engineering, The Johns Hopkins University, Baltimore, Maryland 21218

(Received 14 February 1996; accepted 1 July 1996)

Earlier publications describe the counterflow diffusion flame burner and its unique capability to produce oxide particles having certain structures, such as spheres of one material coated with another, spheres of one composition with attached bulbs of another composition, and uniform multicomponent mixtures. Here we describe the production and properties of bulk quantities of powders produced using this burner. Measurements were made of specific surface area and, for titania, of phase composition. It was found that the controls over powder characteristics used in other forms of flame-synthesis are equally effective in the counterflow diffusion flame burner. We found that the specific surface area of both silica and titania powders decrease with increasing precursor concentrations. Transmission electron microscopy analysis of the titania powders indicates that the mean size of the particles that comprise these powders increases with increasing concentration. These trends are consistent with the collision-coalescence theory of particle growth. In addition, the crystalline phase of titania can be controlled by selecting the appropriate feed stream. For example, over the ranges $TiCl_4$ precursor concentrations tested, feeding it only into the *oxidizer* stream yields mainly *anatase* TiO_2 powders, while feeding only into the *fuel* stream yields mainly *rutile* TiO_2 powders. These trends can be explained by the known atmosphere-dependent anatase-rutile transformation. The present data demonstrate that, in addition to its unique capability to produce certain particle shapes and morphologies, the counterflow diffusion flame burner can be manipulated to produce either of the major commercial titania phases, and also silica, with a wide range of specific surface areas.

I. INTRODUCTION

Titania and silica powders are used to produce paint opacifiers, catalysts, catalyst supports, ceramic membranes, fiber optics, liquid thickeners, varistors, capacitors, etc. New processes are needed to produce these powders at lower cost and without the environmentally detrimental side streams generated by traditional methods. For most applications, a specific particle size, morphology, or crystalline structure is required. For example, for use as light-scattering pigments, *rutile* (one of the crystalline forms of TiO_2) particles with a narrow size distribution around 200 nm are desired.[1] In catalysis, on the other hand, *anatase* (another TiO_2 crystalline form) particles coated with a monolayer of vanadium oxide show higher activity and selective oxidation of *o*-xylene than do their rutile counterparts.[2] Hence, any new processes designed to produce these powders must incorporate a means of control over the powders' physical properties.

In previous papers, we described ceramic oxide powders synthesized by adding vapor precursors to the feed stream of a counterflow diffusion burner. We investigated the formation mechanisms of various oxides and mixed oxides, including Al_2O_3–TiO_2, SiO_2–GeO_2, TiO_2–SiO_2, V_2O_5–TiO_2, V_2O_5–Al_2O_3, and VPO.[3–7] Intriguing oxide particle morphologies and compositions were synthesized. For example, we showed that flame temperature, precursor concentration, and residence time could be controlled so as to produce, in one step, spheres of one material coated with another, spheres of one composition with attached bulbs of another composition, and uniform multicomponent mixtures. These studies and others[8–10] have concentrated on the *in situ* measurement of particle synthesis in counterflow diffusion flames. We report here further progress in counterflow diffusion flame (CDF) synthesis, focusing on use of the burner for mass production of oxide materials. The initial goal was to investigate the degree of control that can be achieved over the oxides' *bulk* properties. To that end we designed

[a]Present address: Microgravity Ventures, Space Systems/Loral, Mail Stop G19, 3825 Fabian Way, Palo Alto, California 94303-4604.
[b]Present address: Gaz de France, DR-CERSTA, 361 Avenue du President Wilson, BP 33, 93211 La Plaine Saint-Denis Cedex, France.
[c]Author to whom correspondence should be addressed.

and built a nonobtrusive powder collector that enables us to collect and analyze bulk amounts of powder. Experimental data on titania and silica powder are reported, which include the dependence of specific surface area and crystal phase on precursor feedstream composition. Results of preliminary transmission electron microscopy analysis of these powders also are reported.

II. EXPERIMENTAL METHOD

A. Counterflow diffusion flame burner

Except for the powder collector to be described here, details of the counterflow diffusion flame burner have been published previously.[11,12] The burner consists of two vertically opposed tubes of rectangular cross section separated by 15 mm. The fuel (H_2, 99.99%, diluted with Ar, 99.998%) flows upward from the lower tube, and the oxidizer (O_2, 99.6%, diluted with Ar, 99.996%) flows downward from the upper tube (see Fig. 1). For convenience, we call the set of gas flow rates that produce a given temperature profile in the burner a "Flame." A single Flame was used in this study; it has been designated as Flame #3 in earlier publications. A visible flame is generated in the burner mouth, i.e., the region where the two opposed gas streams impinge. This flame is very flat and uniform in a horizontal plane. The temperature of the flame can be adjusted through the amount of argon fed to the fuel and oxidizer streams. The temperature profile in the vertical direction is shown in Fig. 2, where −7.5 mm represents the bottom or fuel edge of the mouth, 0 mm the geometric center, and +7.5 mm the top or oxidizer side of the mouth. These

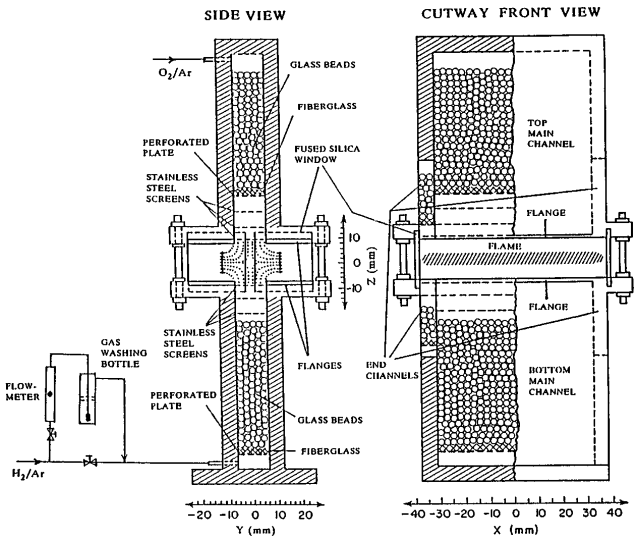

FIG. 1. The counterflow diffusion flame burner. Note the *X*, *Y*, and *Z* coordinate scales; their zero values are at the geometric center of the burner.

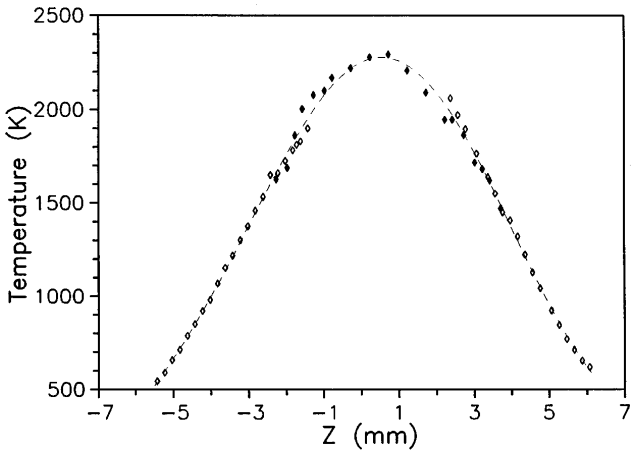

FIG. 2. Temperature profile as a function of height in the burner.

temperatures were measured by two techniques: above 1500 K, by measuring the rotational fine structure in the UV absorption spectra of OH radicals, and from it determining their rotational temperatures; below 2000 K, by using silica coated Pt-Pt 100% Rh thermocouples.

Oxide precursors, which are liquid at room temperature, are added to the flame by bubbling a small part of either the fuel or oxidizer stream (either hydrogen diluted with argon or oxygen diluted with argon) through gas washing bottles containing them. Precursor concentrations are calculated using their known vapor pressures and measurements of the ambient temperature and gas flow rate. By concentration, we mean the ratio of moles of precursor to moles of all gases in that feed stream. In this study, $TiCl_4$ and $SiCl_4$ were used as precursors.

When the metal chloride precursor enters the flame region, it reacts with the oxygen present either as oxygen molecules (O_2), oxygen radicals ($O^{\cdot}$), hydroxyl radicals ($OH\cdot$), or water molecules (H_2O). The resulting metal oxide vapor molecules then begin to condense into particles through the collision-coalescence process, discussed in detail in Sec. IV.

In counterflow diffusion flames, oxide particles are subjected to two competing forces: viscous drag forces due to the gas flow, and thermophoretic forces due to the sharp temperature gradient. Operating conditions can be selected so that, at one or several locations in the flame, the vertical component of the particle thermophoretic velocity is equal to the vertical component of the local gas velocity but of opposite sign.[13,14] At such locations, particles have zero mean vertical speed. The location where this occurs is referred to as a *particle* stagnation plane (PSP). Particles are swept out of the burner (laterally) at a PSP. The PSP is an important factor in determining the temperature-time history the particles experience in the flame. The PSP also marks the location where particles can be captured as they exit the burner.

B. Powder collector

A powder collector was constructed that unobtrusively captures and dilutes the hot aerosol as it leaves the burner at a particle stagnation plane. This collector, shown in Fig. 3, is placed at the mouth of the burner. A diaphragm pump draws in the hot aerosol from the flame into it. The aerosol is quickly cooled and diluted by the addition of cool nitrogen in the main chamber of the powder collector. In this way, the unique particle shapes and crystal phases created in the burner are preserved, the collision rate (between particles) is drastically reduced, and further formation of hard agglomerates is prevented. In addition, the diluted nanoparticle/gas mixture can conveniently be sent to gas-borne particle characterization instruments, electron microscope sampling probes, light scattering cells, etc. Finally, the degree of dilution can be adjusted so as to prevent the condensation of water or other condensibles onto the powder during collection. The rate at which gases are drawn into the powder collector is exactly matched to the flow rate of gases leaving the burner. In this way the flame is not disturbed, and the collection is completely unobtrusive.

The design of the collector ensures that it meets the following performance objectives: Flow into the powder collector does not disturb the flame in any way; thermophoretic deposition within the collector is kept to a minimum. Nitrogen gas flows into the powder collector through the dilution gas feed tube (see Fig. 3). It fills a chamber within the mixing block, and flows out of a slot formed by the mixing block and the rear portion of the front duct. (The slot has two short vertical sections not seen in the cross section in Fig. 3; the slot, therefore, surrounds the incoming hot aerosol.) The narrowness of the slot and the high flow rate of dilution gas (typically ten times the flow rate of gas entering the collector) produce a turbulent sheath of nitrogen that surrounds and quickly mixes with the hot aerosol as it moves into the rear duct. The rear duct is long enough to ensure complete mixing and to prevent the flow into the single exit tube from affecting the flow near the mixing block. The sheath flow reduces thermophoretic deposition of aerosol onto the walls of the rear duct by physically separating the hot aerosol from the walls and by quickly cooling it to reduce the temperature gradient. Even though the dilution gas is introduced through a single feed tube, the slot is narrow enough (relative to the chamber) to ensure that the sheath flow is uniform all around the collector. Therefore, the flow rate of gases into the entrance of the front duct is largely independent of its position along the *x*-direction, except for boundary regions near the left and right edges of the front duct. Furthermore, the sheath is created some distance back from the entrance of the front duct and is aimed away from the flame. This ensures that the flow at the entrance to the front duct is steady and laminar, and does not disturb the flame. Finally, the rate at which gases are drawn into the powder collector is exactly matched to the flow rate of gases leaving the burner. One can easily detect that this is so because the position of the visible part of the flame is unaltered when the matching is perfect.

In these experiments, particles in the diluted and cooled aerosol were collected on two 47 mm diameter Nuclepore filters with a 0.2 μm pore size, held in Teflon holders arranged in parallel (see Fig. 4). Pumping was provided by a dual-chamber GAST diaphragm pump. The pump flow rate fell off as powder accumulated on the filters. Therefore, the nitrogen flow rate frequently was adjusted to ensure that the powder collector maintained a constant dilution factor. As a result, the flow rate entering the powder collector gradually decreased. After the collection run, the powder was gently scraped from the filters using a Teflon scraper, placed in clean glass bottles, and dried overnight at 130 °C in ambient air. Samples typically lost less than 1% of their mass during drying, indicating that these were well-dried powders as collected.

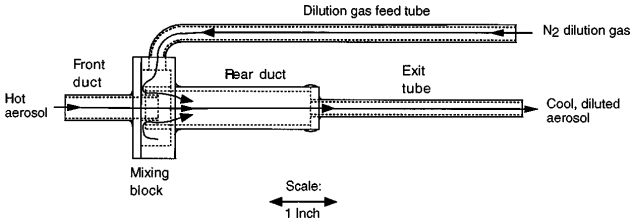

FIG. 3. Scale drawing of the powder collector. Nitrogen gas is used to dilute and cool the aerosol as it exits the flame. The diluted and cooled aerosol is then drawn out through the exit tube.

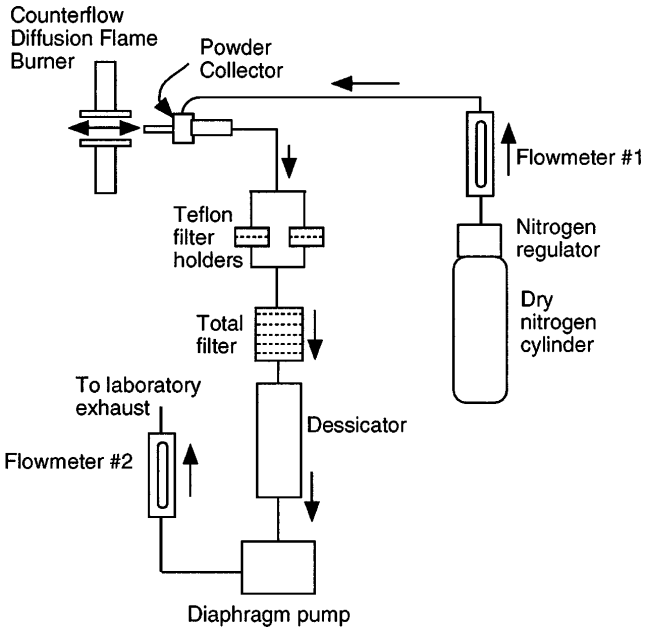

FIG. 4. Schematic of the powder synthesis and collection system.

C. Powder phase and specific surface area measurements

The powder phase was determined by x-ray powder diffraction, using a Philips PW 1729 x-ray generator, PW1820 diffractometer, PW 1710 diffractometer control, and a Digital Microvax 3100. Samples were fixed on 1 in. square glass slides using a 4% solution of Formvar resin in ethylene dichloride. Diffraction patterns were measured from 20 to 80° (2θ). This range was enough to ensure that the major anatase and rutile peaks would be detected.

The specific surface area of powder samples was measured by nitrogen adsorption/desorption in a Micromeritics Flowsorb II 2300. Before measurement, samples were further dried at 120 °C under a flowing mixture of nitrogen and helium for at least 30 min. No measurable mass loss occurred during drying in the Flowsorb apparatus.

D. Microscopy

Ten milliliter powder dispersions were prepared by ultrasonifying powder at 10 mg of powder per liter of purified water. Carbon-coated copper transmission electron microscope grids were briefly dipped into the dispersions and allowed to dry. These were then examined under a Philips EM420ST transmission electron microscope.

III. RESULTS

We will present results for four feed configurations in Flame #3: (i) $TiCl_4$ in the fuel stream, (ii) $TiCl_4$ in the oxidizer stream, (iii) $SiCl_4$ in the fuel stream, and (iv) $SiCl_4$ in the oxidizer stream. In each feed configuration, several precursor concentrations were tested.

Figure 5 shows results for SiO_2. When feeding in either the fuel or oxidizer stream, the specific surface area (σ) decreased with increasing precursor concentration. For the oxidizer stream, the specific surface area decreased from about 125 to 65 m^2/g as the precursor volume concentration increased from 0.06 to 1.20%. A curve fit to these data (shown in Fig. 5) shows that the specific surface area is proportional to the precursor volume concentration to the -0.23 power.

For the fuel stream, the specific surface area decreased from 140 to 100 m^2/g as the precursor volume concentration increased from 0.06 to 1.20%. A curve fit to these data (shown in Fig. 5) shows that the specific surface area is proportional to the precursor volume concentration to the -0.13 power.

Figure 6 shows results for TiO_2. When $TiCl_4$ was fed in the oxidizer stream, the specific surface area decreased from 47 to 25 m^2/g as the precursor concentration increased from 0.03 to 0.23%. A curve fit to these data (shown in Fig. 6) shows that the specific surface area

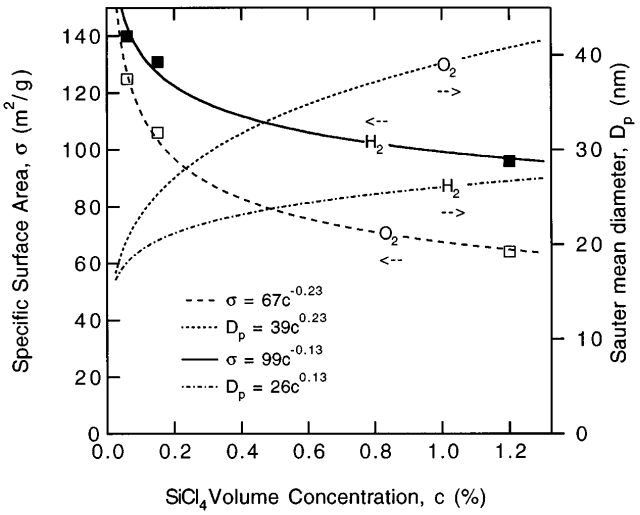

FIG. 5. Specific surface area and Sauter mean diameter of silica versus precursor concentration. Two sets of data are shown: one for precursors in the fuel stream (indicated by H_2), and one for precursors in the oxidizer stream (indicated by O_2).

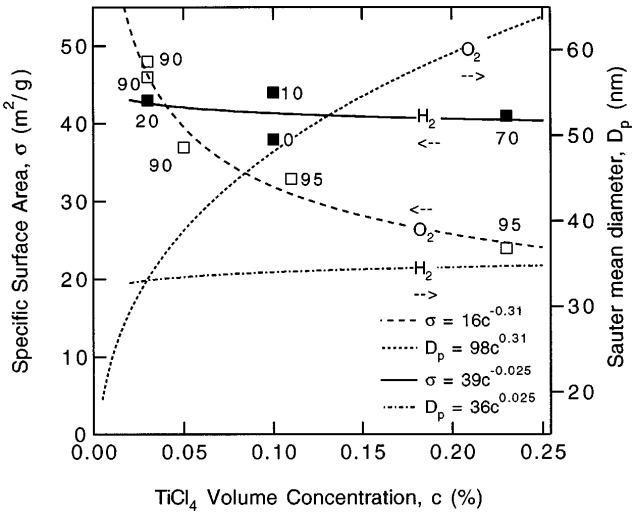

FIG. 6. Specific surface area, Sauter mean diameter, and phase of titania versus precursor concentration. Two sets of data are shown: one for precursors in the fuel stream (indicated by H_2), and one for precursors in the oxidizer stream (indicated by O_2). The numerals next to the data points give the weight fraction of anatase in the collected powders.

is proportional to the precursor volume concentration to the -0.31 power. The powder was 90% anatase for precursor volume concentrations of 0.03% and 0.04% and 95% anatase at a precursor volume concentrations of 0.10% and 0.23%.

When feeding $TiCl_4$ in the fuel stream, the specific surface area remained roughly constant (within experimental error) as the volume precursor concentration increased from 0.03 to 0.23%. A curve fit to these data (shown in Fig. 6) shows that the specific surface area is

proportional to the precursor volume concentration to the −0.025 power. The powder was 80% rutile for precursor concentrations of 0.03%, between 90% and 100% rutile at a precursor concentration of 0.10%, but was only 30% rutile at a precursor concentration of 0.23%.

Figures 5 and 6 also show the Sauter mean diameters $D_p = 6/(\rho_p \sigma)$ (the diameter of a sphere having the same surface to mass ratio and material density as the powder) calculated from the fitted σ vs c curves using $\rho_p = 2.3$ g/gm^3 for silica, 3.84 g/cm^3 for anatase, and 4.26 g/cm^3 for rutile. For the case of $TiCl_4$ in the fuel stream, we used $\rho_p = 4.26$ g/cm^3 for the whole curve despite the fact that the phase of the powder varied substantially with precursor concentration; this undercalculates D_p for $c > 0.10\%$. When feeding through either the fuel and oxidizer stream, the Sauter mean diameter of both the silica and titania particles increased with increasing precursor concentration. (The quantitative dependencies are given in Figs. 5 and 6.) The Sauter mean diameter (D_p) of silica particles made by feeding precursor in the oxidizer stream increased from roughly 20 to 40 nm as the precursor concentration increased from 0.06 to 1.20%. When feeding silica precursor in the fuel stream, D_p increased from about 20 to 27 nm over the same range of precursor concentrations. The wider range of D_p for the case of the oxidizer stream reflects the stronger dependence of σ on c. The Sauter mean diameter of titania particles made by feeding precursors in the oxidizer stream increased from about 30 to 60 nm as c increased from 0.03 to 0.23%. When feeding titania precursor in the fuel stream, D_p was nearly constant at 33 nm. As is the case for silica, the wider range of D_p for the case of the oxidizer stream reflects the stronger dependence of σ on c.

We performed a preliminary microscopic inspection of the titania particles. For titania fed to the oxidizer stream at 0.03%, the particles are mostly separate spheres with diameters ranging from 10 to 50 nm, and having a mean diameter of about 25 nm. This roughly agrees with the Sauter mean diameter of 30 nm. At 0.23% in the oxidizer stream, the particles were again mostly spherical, with diameters ranging from roughly 20 to 90 nm, and having a mean diameter of about 65 nm. This, too, roughly agrees with the Sauter mean diameter of 60 nm.

For titania fed to the fuel stream at 0.03%, the particles were separate spheres with diameters ranging from 15 to 60 nm, and having a mean diameter of about 30 nm. This roughly agrees with the Sauter mean diameter of 33 nm. At 0.23% in the fuel stream, the particles were **not** mostly spherical; instead, they were largely aggregated, and it was not possible to assign a mean diameter. The case of 0.23% $TiCl_4$ in the fuel stream produced anomalies in phase as well as size and morphology, as will be discussed next.

IV. DISCUSSION

A. Specific surface area and particle size

As summarized under Results, we observed a reduction of specific surface area (as measured by nitrogen adsorption/desorption) and an increase in particle size (as measured by microscopy) with increasing precursor concentration. The data roughly fit a power law dependence with $\sigma = const. \times c^n$ where n depends on the oxide produced (titania or silica) and the feed stream in which the precursor is carried (oxidizer or fuel). Except for the case of titania in the fuel stream, which is thought to be an anomalous case as discussed below, n is of order −0.1 to −0.3. This result is ubiquitous in flame synthesis of ceramic powders. For example, Formenti *et al.*[15] used a hydrogen-oxygen diffusion flame to produce alumina, ferrite, germania, silicon, titania, vanadia, and zirconia from the metal chlorides. Their device was very similar to the diffusion flame discussed here, although it was not a counterflow burner. Formenti *et al.*'s results show the specific surface area of titania decreased approximately 3.2-fold when the precursor concentration increased approximately 43-fold. This fits a power law dependence with precursor concentration raised to the −0.3, which is similar in magnitude to the present results for silica and titania.

Similarly, George *et al.*[16] studied the formation of titania from $TiCl_4$ in a premixed $CO + O_2 + N_2$ flame. They found that the particle diameter varied with precursor concentration to the 0.33 to 0.38 power. The specific surface area of their powders would, therefore, vary with precursor concentration roughly to the −0.3 to −0.4 power, which also is similar to the present results.

The experimentally observed inverse relation between specific surface area and precursor concentration indicates that the primary mechanism of particle growth in the flame is the so-called collision-coalescence process, studied in detail by Ulrich.[17] Particle formation is initiated when the chemical precursors react in the flame and form metal oxides. Since the equilibrium vapor concentration of these oxides at the temperatures found in the flame is much lower than their ambient concentrations, they quickly begin to form particles by colliding and adhering to one another. The particles thus formed collide with one another, in turn forming progressively larger particles. If the temperature is high enough, the particles coalesce after colliding, remaining compact in form as they grow. This so-called collision-coalescence process continues until the particles move out of the flame into regions too cool to allow coalescence following the collisions.

The interparticle collisions are caused by Brownian motion. Hydrodynamically, flame-synthesized particles often fall within the free-molecular regime throughout the entire growth process. Ulrich solved the particle

balance equations for that case and found that, for a given growth period, the specific surface area of the aerosol varies with the initial concentration of molecular oxide to the −0.4 power. The order of magnitude of the predicted dependence agrees with the experimental observations summarized above. Furthermore, other researchers have shown that Ulrich's solution also correctly predicts the size *distribution* of particles.[16] Thus there is strong evidence indicating that the collision-coalescence process is the operating mechanism for particle growth in flames, and the counterflow diffusion flame appears to be no exception.

Another result from Ulrich's analysis is that the final particle size distribution resulting from the collision-coalescence process is not dependent on the size distribution present shortly after reaction of the precursor. Rather, the final size distribution depends on the total concentration of material present, the total formation time (i.e., the residence time in the flame), and the Brownian coagulation coefficients. Therefore, details of the beginning stages of particle formation are irrelevant to the final particle size distribution. This result is important since it simplifies the analysis of particle growth by eliminating consideration of nucleation processes that may or may not occur immediately after reaction of the precursor.

The results for titania produced by feeding titanium tetrachloride in the fuel stream do not follow the same trends as the results for the other feed configurations. The specific surface area varies with precursor concentration to the −0.03 power—a very weak dependence compared to the other powders. Also, the micrographs show that, unlike the other powders, the particles are not individual spheres. Rather, they are branched agglomerates of many smaller particles. One possible explanation for these results is connected with the fact that the flame was much more luminescent for the case of $TiCl_4$ in the fuel stream than for the other feed configurations. The luminescence is the result of the particles thermally radiating at high temperatures in the flame. The thermal radiation certainly cools the flame, although the magnitude of this effect is not known, and no attempt was made to measure the flame temperature in this feed configuration. A lower flame temperature would result in less complete coalescence of particles after collisions, leading to the branched particle morphology and high specific surface area.

B. Titania phase

Two main phases of titania are produced by flame synthesis: anatase and rutile. Both anatase and rutile possess a tetragonal structure, but in anatase, the oxygens are in a distorted face-centered cubic arrangement, and in rutile the oxygens are in a distorted hexagonal arrangement.[18] Anatase has a more open structure than rutile; its density at 25 °C is 3.84 g/cm^3 compared to rutile's 4.26 g/cm^3. Although rutile is thermodynamically more stable than anatase, anatase is readily formed at low temperatures due to its relatively fast crystallization kinetics. For example, wet chemical processes invariable produce anatase.[19,20] Relatively low-temperature flame processes also produce anatase.[11,21,22]

Formation of rutile from anatase requires substantial atomic rearrangement that is facilitated by high temperatures. The transformation requires about 8 h at 500 to 600 °C, but requires only a second at 1200 °C.[17,18,23]

The rate of transformation of anatase to rutile increases with temperature as described above, but it also increases with increasing concentration of oxygen vacancies within the crystal. The concentration of oxygen vacancies increases with decreasing ambient oxygen concentration. Therefore, the rate of transformation of anatase to rutile increases with decreasing ambient oxygen concentration. This trend has been demonstrated by experimenters who heated powder in a platinum boat under various atmospheres.[24,25]

The phase of the produced powder depends on the extent of transformation, which in turn depends on the rate of transformation and on the processing time. As a result, the phase of the flame-synthesized powder can be controlled through those factors that control the rate of transformation and the processing time.

The counterflow diffusion burner is ideally configured to control phase using the ambient oxygen concentration. A high ambient oxygen concentration is available by feeding precursors in the oxidizer stream, while a low oxygen concentration is available by feeding precursors in the fuel stream. The present results show that, as expected, rutile is obtained when using the fuel stream, while anatase is obtained while using the oxidizer stream. The lack of rutile in powders formed on the oxidizer stream is probably due to the relatively high concentration of gaseous oxygen, which leads to a low concentration of the oxygen vacancies that are necessary for phase transformation to occur. Conversely, on the fuel side, there is a lower concentration of gaseous oxygen, which allows the formation of substantial numbers of oxygen vacancies that promote the transformation of anatase to rutile.

An anomalous effect is seen at the highest precursor concentration on the fuel side. The powder formed using 0.23% $TiCl_4$ in the fuel stream is only 30% rutile. This may have been due to a reduction in flame temperature caused by radiative cooling of the particles, as described in connection with the specific surface area data. A lower flame temperature would result in more sluggish transformation from anatase to rutile.

V. CONCLUSIONS

We have reported the results of experiments on the synthesis of titania and silica in a counterflow diffusion

flame burner. Earlier publications describe the unique capability of the counterflow diffusion flame burner to produce oxide particles having certain structures and compositions. Here we have described the production and properties of *bulk* quantities of silica and titania powders produced using the same burner.

We described a powder collector that unobtrusively cools and dries the aerosol as it exits the flame, and collects the powder on filters.

Nitrogen adsorption/desorption measurements show that the specific surface areas of the silica and titania powders are inversely proportional to the precursor concentration, in accordance with the collision-coalescence theory of aerosol formation. According to the theory, the specific surface area of the powder exiting the flame depends on the precursor concentration, the residence time, and the temperature dependent Brownian coagulation coefficients, but is independent of the particle size distribution that exists immediately after reaction of the precursor. Therefore, the nucleation process that may or may not occur at the start of the particle formation does not affect the properties of the final powder.

A microscopic study shows that the particles that comprise the powders are spherical, and their diameters roughly agree with the Sauter mean diameter calculated from the specific surface areas.

Powder diffraction measurements show that the phase of the titania powder was affected by the composition of the feed stream. Anatase powders were produced by feeding $TiCl_4$ in the oxidizer stream, while rutile powders were produced by feeding in the fuel stream. This is in accordance with the known atmospheric-dependent anatase to rutile transformation, which occurs more rapidly as the ambient oxygen concentration decreases.

The above results held throughout the range of precursor concentrations and feed configurations tested, except for the case of $TiCl_4$ in the fuel stream, which showed anomalous behavior. This may have been due to reduced flame temperature caused by radiative cooling of titania particles, which emitted particularly bright thermal radiation in this feed configuration.

The counterflow diffusion flame process allows one to produce powders of controllable phase and specific surface area. This makes it an ideal technology for producing the ceramic powders needed to manufacture paint opacifiers, catalysts, catalyst supports, ceramic membranes, fiber optics, liquid thickeners, varistors, capacitors, and other products yet to be developed.

ACKNOWLEDGMENTS

The work was supported by the Division of Materials Sciences, Office of Basic Energy Sciences, U.S. Department of Energy via Grant DE-FG02-88ER45356.

REFERENCES

1. J. H. Braun, A. Baidins, and R. E. Marganski, Prog. Org. Coat. **20**, 105 (1992).
2. G. C. Bond and S. F. Tahir, Appl. Catal. **71**, 1 (1991).
3. C-H. Hung and J. L. Katz, J. Mater. Res. **7**, 1861 (1992).
4. C-H. Hung, P. F. Miquel, and J. L. Katz, J. Mater. Res. **7**, 1870 (1992).
5. J. L. Katz and P. F. Miquel, Nanostructured Mater. **4**, 551 (1994).
6. P. F. Miquel, C-H. Hung, and J. L. Katz, J. Mater. Res. **8**, 2404 (1993).
7. P. F. Miquel and J. L. Katz, J. Mater. Res. **9**, 746 (1994).
8. M. R. Zachariah, D. Chin, H. G. Semerjian, and J. L. Katz, Appl. Opt. **28**, 530 (1989).
9. M. R. Zachariah and R. G. Joklik, J. Appl. Phys. **68**, 321 (1990).
10. M. R. Zachariah, *Chemistry of silane oxidation and pyrolysis during particle formation: Comparison with in situ measurements*, Proceedings of the Western States Section of the Combustion Institute, March 1991 Meeting.
11. S. L. Chung and J. L. Katz, Combustion and Flame **61**, 271 (1985).
12. J. L. Katz and C. H. Hung, U.S. Patent 5 268 337.
13. A. Gomez and D. E. Rosner, Combustion Sci. Technol. **89**, 335 (1993).
14. P. F. Miquel, *Flame Synthesis of Nanostructured Mixed Oxides and Its Application to the Formation of Catalysts*, Ph.D. Thesis, The Johns Hopkins University, Baltimore, MD (1995).
15. M. Formenti, F. Juillet, P. Meriaudeau, S. J. Teichner, and P. Vergnon, in *Aerosols and Atmospheric Chemistry*, edited by G. M. Hidy (Academic Press, New York, 1972), p. 45.
16. A. P. George, R. D. Murley, and E. R. Place, in *Fogs and Smokes*, Symposium of the Faraday Society (Chemical Society, London, 1973), p. 63.
17. G. D. Ulrich, Comb. Sci. Tech. **4**, 47–57 (1971).
18. R. D. Shannon and J. A. Pask, Am. Minerol. **49**, 1707 (1964).
19. S. Hishita, I. Mutoh, K. Koumota, and H. Yanagida, Ceram. Int. **9**, 61 (1983).
20. K. J. D. Mackenzie and P. J. Melling, Trans. J. Brit. Ceram. Soc. **73**, 23 (1974).
21. A. Kobata, K. Kusakabe, and S. Morooka, AIChE J. **37**, 347 (1991).
22. M. K. Akhtar, Y. Xiong, and S. E. Pratsinis, AIChE J. **37**, 1561 (1991).
23. K. P. Kumar, V. T. Zaspalis, F. F. M. De Mul, K. Keizer, and A. J. Burggraff, in *Better Ceramics Through Chemistry V*, edited by M. J. Hampden-Smith, W. G. Klemperer, and C. J. Brinker (Mater. Res. Soc. Symp. Proc. **271**, Pittsburgh, PA, 1992), pp. 499–504.
24. Y. Iida and S. Ozaki, J. Am. Ceram. Soc. **44**, 120 (1961).
25. R. D. Shannon and J. A. Pask, J. Am. Ceram. Soc. **48**, 391 (1965).